Research Article

Ahmed J. Jasim, Ghassan M. Sulaiman*, Hilal Ay, Salman A. A. Mohammed, Hamdoon A. Mohammed*, Majid S. Jabir, and Riaz A. Khan*

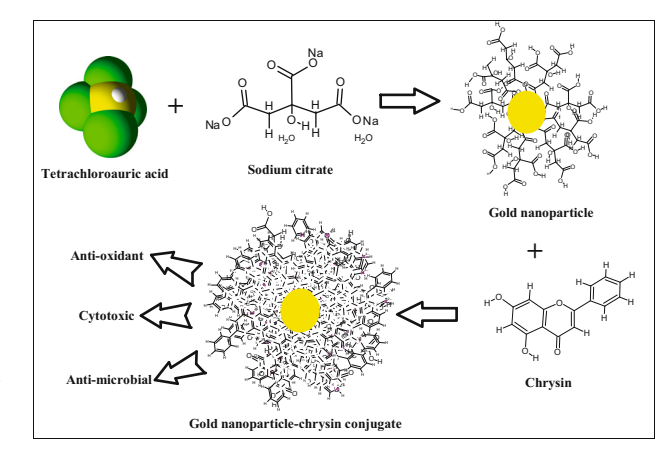
Preliminary trials of the gold nanoparticles conjugated chrysin: An assessment of antioxidant, anti-microbial, and *in vitro* cytotoxic activities of a nanoformulated flavonoid

https://doi.org/10.1515/ntrev-2022-0153 received January 17, 2022; accepted June 25, 2022

Abstract: Chrysin (CHR), a dihydroxy flavone, exhibits several bioactivities, *i.e.*, anti-oxidant, anti-inflammatory, and anti-cancer, and is known to possess limited aqueous solubility causing lowered bioavailability, and compromised therapeutic efficacy. Gold nanoparticles (AuNPs) conjugated chrysin (CHR–AuNPs) were prepared and characterized by UV-Vis, Fourier transform infra-red, X-ray diffraction, energy dispersive X-ray (EDX), and zeta potential analyses. The nanoformulated CHR–AuNPs were primarily examined on trial scale for their cytotoxic, anti-oxidant, and anti-microbial activity in comparison to the unformulated CHR. The CHR–AuNPs effectively scavenged the 2,2-diphenyl-1-picrylhydrazyl free radicals, also in comparison to CHR and AuNPs. The CHR–AuNPs also exhibited potential cytotoxic effects in a dose-dependent manner and

Hilal Ay: Department of Molecular Biology and Genetics, Faculty of Science and Arts, Ondokuz Mayis University, Samsun, 55139, Turkey Salman A. A. Mohammed: Department of Pharmacology and Toxicology, College of Pharmacy, Qassim University, Qassim 51452, Saudi Arabia

Majid S. Jabir: Department of Applied Sciences, Division of Biotechnology, University of Technology, Baghdad, Iraq



Graphical abstract

demonstrated significant reduction (P = 0.05) of the cells proliferation, and growth of the human breast cancer cell lines, AMJ13, which were measured by 3-(4,5-dimethylthiazal-z-yl)-2,5-diphenyltetrazolium, and crystal violet assays, respectively. When compared with the pure CHR and free-AuNPs, the CHR-AuNPs exerted highest anti-microbial bioactivity against *Staphylococcus aureus* and *Escherichia coli*. The strong anti-oxidant, anti-microbial, as well as cytotoxic activity of the CHR-AuNPs preparation has the potential for clinical use after considerable appropriate developments.

Keywords: chrysin, chrysin-nano, gold nanoparticles, chrysin-conjugated nanoparticles, anti-oxidant, anti-microbial, anti-cancer, cytotoxicity, AMJ13 cell lines

1 Introduction

Cancer, the state of uncontrolled cells proliferation, is a significant health problem all over the world, and more than 11 million people have been diagnosed with various cancer types [1]. It is estimated that by 2025, breast cancer

^{*} Corresponding author: Ghassan M. Sulaiman, Department of Applied Sciences, Division of Biotechnology, University of Technology, Baghdad, Iraq, e-mail: ghassan.m.sulaiman@uotechnology.edu.iq

^{*} Corresponding author: Hamdoon A. Mohammed, Department of Medicinal Chemistry and Pharmacognosy, College of Pharmacy, Qassim University, Qassim 51452, Saudi Arabia; Department of Pharmacognosy and Medicinal Plants, Faculty of Pharmacy, Al-Azhar University, Cairo 11371, Egypt, e-mail: ham.mohammed@qu.edu.sa

^{*} Corresponding author: Riaz A. Khan, Department of Medicinal Chemistry and Pharmacognosy, College of Pharmacy, Qassim University, Qassim 51452, Saudi Arabia, e-mail: ri.khan@qu.edu.sa Ahmed J. Jasim: Department of Biomedical Engineering, University of Technology, Baghdad, Iraq

³ Open Access. © 2022 Ahmed J. Jasim *et al.*, published by De Gruyter. © This work is licensed under the Creative Commons Attribution 4.0 International License.

cases will rise to 19 million. In addition, cancer is the most common cause of death, due to factors, such as poor oral absorption and diminished biodistribution of the chemotherapeutic agents. The adverse effects of conventional treatments, *i.e.*, chemotherapy, radiotherapy, and surgery combined co-therapies are insufficiently effective [2]. As a result, new treatment modules with the enhanced oral absorption or facilitated systemic delivery, higher bioavailability, and better biotransport stability are required. Newer strategies for delivering the developed therapeutic modules with site-specificity and appropriate trigger release of the chemotherapeutic agents to tumor cells are a priority [3]. Recently, nanotechnology-based diagnosis and therapy systems have been developed for the majority of cancers treatment approaches [4]. The multifunctional nanosystems are among the most recent developments. Several strategies have been technologically advanced to selectively deliver these anti-cancer drugs to cancer lesions [5]. The majority of these strategies rely on the tumor microenvironment's distinct biological and physical characteristics, which are manipulated to outreach to the cancer cells. Recently, special emphasis has been placed on the link between inflammation and the development of cancer cells in patients with stabilized (non-metastatic) cancers [6].

Nanomedicine, the nanotechnology branch dealing with the development of drugs and their delivery systems at the nanoscale, is a promising theranostic tool taking care of diagnosis and therapy as well. Recent breakthroughs in the utilization of nanoparticles (NPs) have also offered the renewed potential to dispense anti-cancer drugs to particular tissues with dose accuracy, therapeutic effectiveness, and safety [7,8]. The gold nanoparticles (AuNPs) have shown distinctive properties, and their numerous surface functions have made them one of the choices for a nanoscale particle for use in nanomedicines. These NPs are biocompatible and have a large surface-tovolume ratio which is considered enough for loading higher concentrations of single or multiple drugs for site delivery. The AuNPs have been utilized in a wide range of biotechnological applications, notably in drug delivery systems [9,10]. The AuNPs based therapeutic modules have been reported to have superior outcomes over conventional cancer treatment modalities due to their competitive performance as drug carriers [11].

Epidemiological studies concerning the roles of flavonoids in the healthcare system have confirmed that people with diets high in flavonoid products are less likely to develop cancer and some other chronic diseases [12]. There is also a growing interest in using flavonoidrich plant-based products, as well as pure flavonoid

compounds, as nutritional supplements in the treatment and prophylactics of cancer, metabolic disorders, cardiovascular diseases, and coronary disorders [12]. Flavonoids are poly-hydroxylated compounds with the molecular framework of the three cyclic structures, $C_6-C_3-C_6$ carbons arrangement. The number and distribution of the hydroxyl groups attached to the flavonoid framework seem to play important role in the biological activities elicitations of these flavonoid classes of compounds [13]. Among these, chrysin (CHR) is one of the interesting anti-cancer compounds, which is chemically identified as 5,7-dihydroxyflavone [13]. CHR has been reported to possess several biological activities, and certain therapeutic potentials of this compound are confirmed. The anti-cancer activity of CHR has been established, and its role in the limitation of breast, ovarian, cervical, gastric, bladder, lungs, and prostate cancers have been reported [14]. Unfortunately, the poor bioavailability of CHR associated with its meager aqueous solubility and aqueous dispersion is a reason for its limited clinical applications [15], and this has led to devise suitable delivery systems for CHR-containing formulation [15,16]. which needs to be a highly active tissue-targeted drug delivery system that can be synthesized from a wide range of materials, including inorganic NPs [17]. The NP-based therapy and drug delivery systems have the potential to provide a better outcome as a combination therapy. The AuNPs may outperform monotherapy in improving the efficacy and biocompatibility of a cancer therapeutic agent [18]. In this study, CHR was formulated as a gold conjugated nanoparticle (CHR-AuNP) preparation and was investigated as the nanoformulation for anti-oxidant, anti-cancer, and anti-microbial activities in comparison to the pure CHR. The anti-oxidant potential as 2,2-diphenyl-1-picrylhydrazyl (DPPH) free-radical scavenging capacity, cytotoxic activity against triple-negative human breast cancer-derived AMJ13 cell lines, and anti-microbial activity against Gram-positive and Gram-negative microbial strains were evaluated.

2 Materials and methods

2.1 Materials and reagents

CHR (structurally 5,7-dihydroxyflavone; purity ~97%), DPPH, ascorbic acid, ethanol, fetal bovine serum (FBS), and RPMI-1640 medium were obtained from Sigma Chemical Co. (St. Louis, MO, USA). Tetrachloroauric acid trihydrate (HAuCl₄·3H₂O) was obtained from Strem Chemicals (UK), while sodium citrate dihydrate (C₆H₅Na₃O₇·2H₂O), dimethyl

sulfoxide (DMSO), 3-(4,5-dimethylthiazal-z-yl)-2,5-diphenyltetrazolium (MTT), and crystal violet were purchased from Sigma-Aldrich Chemie GmBH (Schnelldorf, Germany). Antibiotics such as penicillin and streptomycin were procured from Biosource International (Nivelles, Belgium). Molar Hinton agar was purchased from Merck, Germany. Double distilled water was obtained from Millipore water purification system. All the other chemicals and reagents used in the experiments were of analytical grade.

2.2 Organisms

AMJ13, human triple-negative breast cancer cell lines were provided by the Biotechnology Research Center, Al-Mustansiriyah University, Baghdad, Iraq. The cells were cultured in sterile Falcon flasks ($T 25 \text{ cm}^2$, USA), and supplemented with RPMI-1640 medium enriched with L-glutamine (2 mM) and FBS (10%, 20 mM) at a condition of 5% of CO₂, 37°C of temperature, and 1 atmospheric pressure.

Clinical isolates, Escherichia coli (Gram negative) and Staphylococcus aureus (Gram positive), were used to evaluate the anti-microbial activity of the prepared formulations. The clinical isolates were provided by the Division of Biotechnology, Department of Applied Sciences, University of Technology, Baghdad, Iraq.

2.3 Preparation of AuNPs

AuNPs were prepared by chemical method. In brief, an agueous solution of HAuCl₄·3H₂O (MW 393.83 amu, 0.1 mM, 10 mL water) was let to boil on a hot plate at atmospheric pressure under stirring, and at the boiling, trisodium citrate (MW 294 amu, 0.3 mM, 15 mL water) was added in one instance, heating was stopped, and stirring continued for overnight at room temperature (22–25°C) [19].

2.4 CHR-AuNPs conjugation

Pure CHR (10 mg) was dissolved in 5 mL of DMSO and stirred at 1,000 rpm for 15 min under room temperature to obtain a homogeneous solution with complete and clear visible solubility [20]. The CHR suspension was added to the solution of AuNPs (1:9 mL) and stirred for 20 h, through overnight at room temperature. The color of

the solution changed to light violet, and the excess CHR was removed by ultracentrifugation (13,000 rpm, 30 min) at the end of the reaction [21]. The percentage of conjugated CHR on the AuNPs were calculated using the following equation:

Drug loading (%) = Weight of chrysin in NPs/Weight of NPs
$$\times$$
 100. (1)

The CHR in vitro release from CHR-AuNPs was performed as previously reported [20] with minor modification. Briefly, 10 mg of CHR-AuNPs was taken in a release medium constituting PBS and DMSO at 37°C under agitation. The pH was set at 7.4, and CHR is released for different periods from 1 to 15 h, after each hour the measurement of the CHR absorbance was recorded by the UV-Vis spectrophotometer. The concentrations of the released CHR from CHR-AuNPs were calculated using the following equation:

Cumulative release ratio (%) =
$$(Wr/Wt) \times 100$$
, (2)

where Wr is the CHR weight in each release and Wt is the weight of CHR-AuNPs taken.

2.5 Characterization of prepared NPs

For Fourier transform infra-red (FT-IR) analysis, a spectrophotometer (8400S, Shimadzu, Japan) with a spectral range from 4,000 to 400 cm⁻¹ and a resolution of 4 cm⁻¹ was used. An X-ray diffractometer was employed to determine the crystalline state of the prepared samples (XRD-6000, Shimadzu, Japan). The diffraction patterns were obtained using the K copper incident beam ($\lambda = 1.542^{\circ}$) at $2 = 20-60^{\circ}$ planes. The X-ray tube had 45 kV voltage and 30 mA current. For field emission scanning electron microscopy (FE-SEM) analysis, MIRA 3 TESCAN was used. To examine the shape and metallic presence, an energy dispersive X-ray analysis (EDX) was performed. The Zeta PALS instrument (UK) was used to measure the zeta potential and particle size [22].

2.6 Cytotoxicity assay

Standard MTT assay was used to evaluate the cytotoxic activity of the AuNPs, CHR, and the CHR-AuNPs nanoformulation against AMJ13 cell lines [23]. The AMJ13 cells were grown and maintained in Falcon® flasks containing RPMI-1640 supplemented with 10% FBS, 100 units/mL penicillin, and 100 µg/mL streptomycin. The cells were passaged twice a week with Trypsin-EDTA, reseeded at 80% confluence, and incubated at 37°C. The cell lines were seeded at a density of 1×10^4 cells/well and treated with AuNPs, CHR, and the CHR-AuNPs formulation at various concentrations after 24 h, or when a confluent monolayer was achieved. After 72 h of treatments, cells viability was assessed by removing the medium, adding 28 µL of 2 mg/mL MTT solution, and incubating the cells for 2.5 h at 37°C. Following the removal of the MTT solution, the crystals in the wells were solubilized by adding 130 µL of DMSO, followed by 15 min of incubation at 37°C with shaking. The absorbance was measured using a microplate reader at 492 nm, and the experiments were repeated thrice. The reduction in cells proliferations (cytotoxicity) was calculated using the following equation:

DE GRUYTER

where Ab control is the absorbance of the control, while Bb is the absorbance obtained for the tested samples.

Crystal violet staining was also used to investigate the viability of the cells in the presence of AuNPs, CHR, and CHR-AuNPs. The cells were seeded into 24-well micro-titration plates at a density of 1×10^5 cells/mL and incubated for 24 h at 37°C to visualize their shape under an inverted microscope [24]. The cells were then treated with the IC₅₀ concentration of AuNPs, CHR, and CHR-AuNPs for 24 h. The plates were stained with crystal violet and incubated for 12 min at 37°C. Then, tap water was used to remove the dye, and the cells were investigated under the microscope at 40× magnification power, where clear images of the cells were captured with a digital camera attached to the microscope [25].

2.7 Anti-oxidant activity

Anti-oxidant activities of AuNPs, CHR, and CHR-AuNPs formulations were measured using DPPH free radicals scavenging method [26]. The tested samples (1 mL in absolute ethanol) at four different concentrations, 1.3, 2.6, 12.5, and 25 µg mL were mixed with 450 µL of DPPH solution. The standard positive control, ascorbic acid (at a concentration of 10 µg/mL), was mixed with DPPH solution in the same manner. The reduction in the DPPH free radicals color in response to the scavenging power of the tested samples and ascorbic acid was measured spectrophotometrically at 517 nm after 30 min of incubation in dark. The anti-oxidant activity of the samples, in terms of

their scavenging effects, was calculated from the following equation:

where Ab control and Ab sample are the absorbance of the control and test samples, respectively.

2.8 Anti-microbial activity

The anti-microbial activities of AuNPs, CHR, and CHR-AuNPs were tested against human pathogens: S. aureus and E. coli. The bacteria were extracted from their stock cultures using a sterile wire loop [27]. To investigate the effects of AuNPs, CHR, and CHR-AuNPs, the growth curves of the bacteria were obtained. The microbial strains were cultured on Molar Hinton agar plates at 37°C, with inoculations of 50 mL of nutrient broth on freshly cultured plates [28]. The bacteria grew until the nutrient broth reached an optical density (OD) of 0.1 at 600 nm, which corresponded to a microbial concentration of 10⁸ CFU/mL. The nutrient broth was then supplemented with NPs, and microbial cultures (1 mL) were added and incubated at 37°C for 12h under slight agitation. Microbial growth was determined using a spectrophotometer by measuring the OD [29].

2.9 Statistical analysis

All the data were analyzed using the unpaired *t*-test, which compared the studying groups at a significant p-value of <0.05. All experiments were performed in triplicate and data were calculated as the mean ± standard deviation.

3 Results

3.1 NPs preparation and CHR conjugation

The AuNPs were prepared by chemical reduction method utilizing trisodium citrate dehydrate and HAuCl₄·3H₂O. A solution of HAuCl₄·3H₂O was reacted with trisodium citrate dihydrate aqueous solution, and the reaction mixture color changed from pale yellow to purple, and finally to red, indicating the preparation of the AuNPs (Figure 1).



Figure 1: Samples: (a) AuNPs preparation, (b) CHR solution, and (c) CHR-AuNPs preparation.

Based on equation (1), the AuNPs conjugation to CHR was 15.2%, and the release kinetics of CHR in physiological pH of 7.4 was performed using UV-Vis spectroscopy (Figure 2). During the early phase of first hour, it was ~25% release, in the second hour the release rate was over 50%. In the sixth hour the (%) release rate reached ~80%. From 6 to 9 h, the release was observed at above 85% and thereafter it stabilized for the rest of the total 15 h of the drug release period during the simulated release experiment. The fast release of the drug was observed from 9 to 15 h at ~85%.

3.2 UV-Vis spectroscopy of prepared NPs

To confirm the formation and binding of AuNPs to CHR, UV-Vis spectrophotometry was used. As seen from Figure 3, the AuNPs' UV-Vis spectrum showed absorption maxima $\lambda_{\rm max}$ at 520 nm. While the CHR, a light yellowish solution,

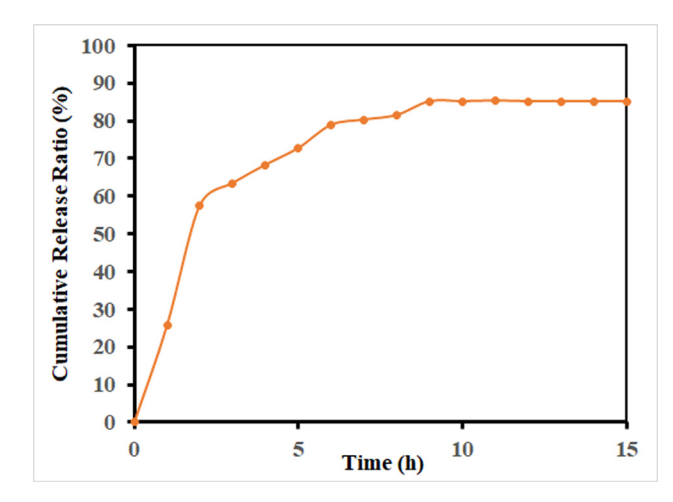
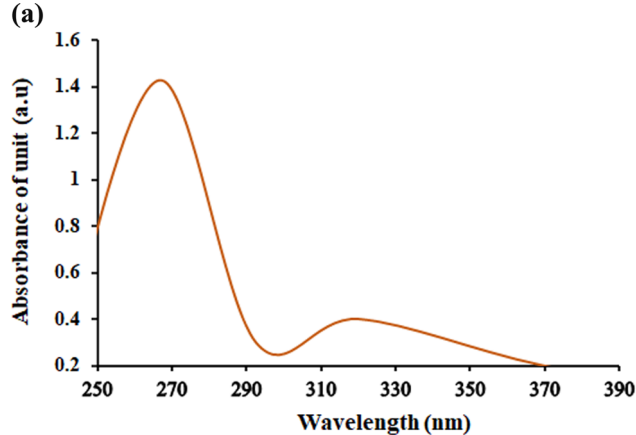
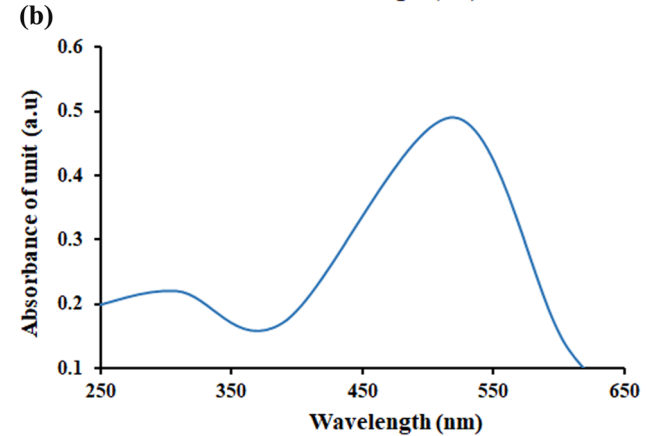


Figure 2: Release profile of CHR from the CHR-AuNPs nanoformulation.





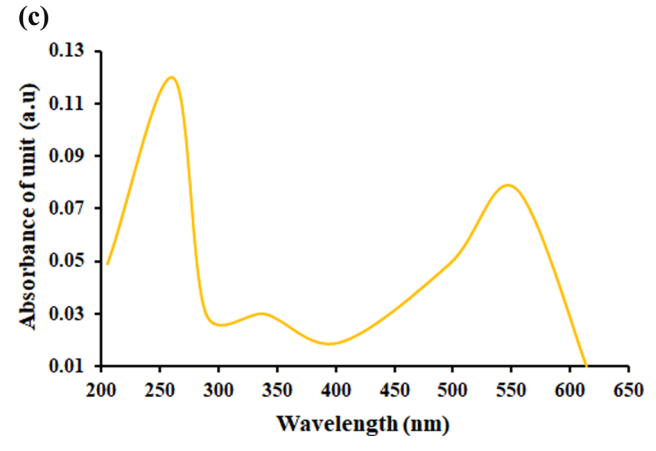
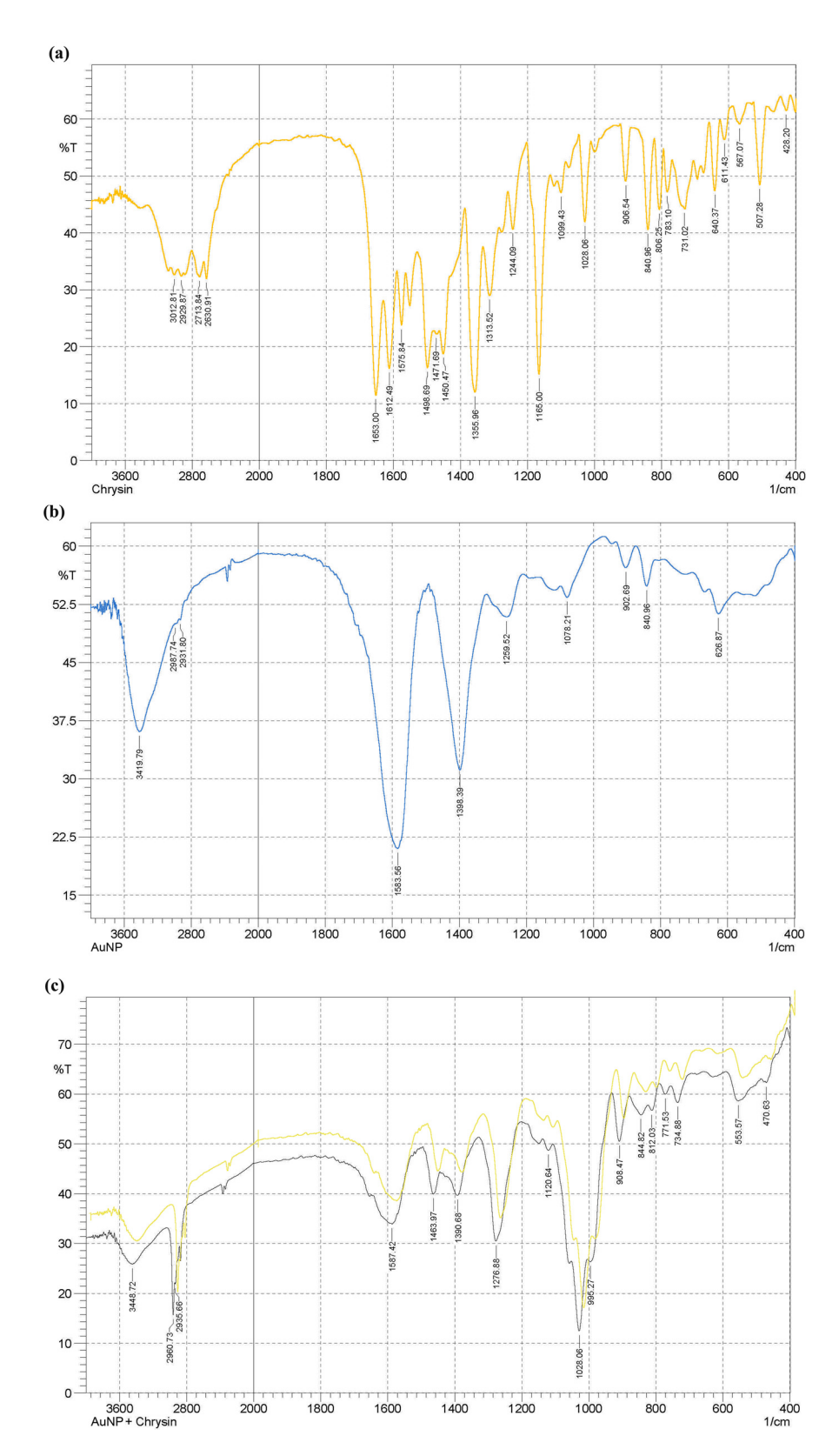


Figure 3: UV-Vis spectroscopic spectra: (a) AuNPs, (b) CHR, and (c) CHR-AuNPs.

showed the UV absorption maxima at $\lambda_{\rm max}$ 268 nm. The absorption maxima for CHR–AuNPs was exhibited at 260 and 550 nm $\lambda_{\rm max}$ values.

3.3 FT-IR spectroscopic analyses

The FT-IR spectrum (Figure 4) of CHR exhibited absorptions at 3012.79 cm⁻¹ (OH), at 2929.87, 2713.84, and



 $\textbf{Figure 4:} \ \textbf{FT-IR} \ \textbf{spectroscopic analyses:} \ \textbf{(a)} \ \textbf{CHR, (b)} \ \textbf{AuNPs, and (c)} \ \textbf{CHR-AuNPs.}$

2630.91 cm⁻¹ (C–H stretchings), and at 1653.00 cm⁻¹ (α,β-unsaturated carbonyl, C=O). The bands at 1355.96 and 1028.06 cm⁻¹ (C–O–C) and 840.96 and 731.02 cm⁻¹ (aromatic character) were observed. The AuNPs-CTT absorptions at 3419.79 cm⁻¹ (O–H stretching), 2987.74 and 2931.80 cm⁻¹ (C–H stretchings), at 1583.56 cm⁻¹ (C=O) group, and at 1398.39 cm⁻¹ (ether function) were observed for the citrate-surface AuNPs. The CHR–AuNPs absorption at 3448.72 cm⁻¹ (O–H), at 2960.73 and 2935.66 cm⁻¹ (CH stretchings), at 1587.42, 1463.97, and 1390.68 cm⁻¹ (aromatic C=C bonds), and 1276.88 cm⁻¹ (C–O stretchings) were observed.

3.4 X-ray diffraction (XRD) analyses

Crystal structures of CHR, AuNPs, and CHR–AuNPs were confirmed by the XRD analysis (Figure 5). The AuNPs' diffraction peaks were observed at 30.56°, 38.12°, 44.18°, and 56.35°, which verified the face-centered polycrystal-line cubic structure. The crystallinity of AuNPs was compared with the available XRD pattern in the database, JCPDS 00-004-0784 [30]. The CHR showed strong 2θ peaks at 7.18°, 12.60°, 14.92°, 17.75°, 92.14°, 27.34°, and 27.68°, indicating a more crystalline structure. When CHR was loaded onto AuNPs, five peaks were observed, *i.e.*, 23.5°, 27.55°, 38.15°, 44.01°, and 57.45°.

3.5 FE-SEM and EDX analyses

FE-SEM images (Figure 6) exhibited relatively spherical shapes of the AuNPs with 17.37–25.90 nm size range. CHR–AuNPs nano-preparation showed spherical, nearly homogenous composition with size ranging between 31.53 and 38.58 nm. The CHR EDX analysis showed the presence of C and O, the AuNPs EDX analysis showed the presence of Au (51.76%, main component), while CHR–AuNPs showed the presence of Au, C, and O elements, as shown in Figure 6; right lane.

3.6 ζ-potential analyses

CHR ζ -potential and mobility were –161.00 and –3.30, respectively. The AuNPs carried –31.54 mV ζ -potential, and the mobility was –2.46, while the CHR–AuNPs carried –48.92 mV ζ -potential, and mobility was –3.82 (Figure 7).

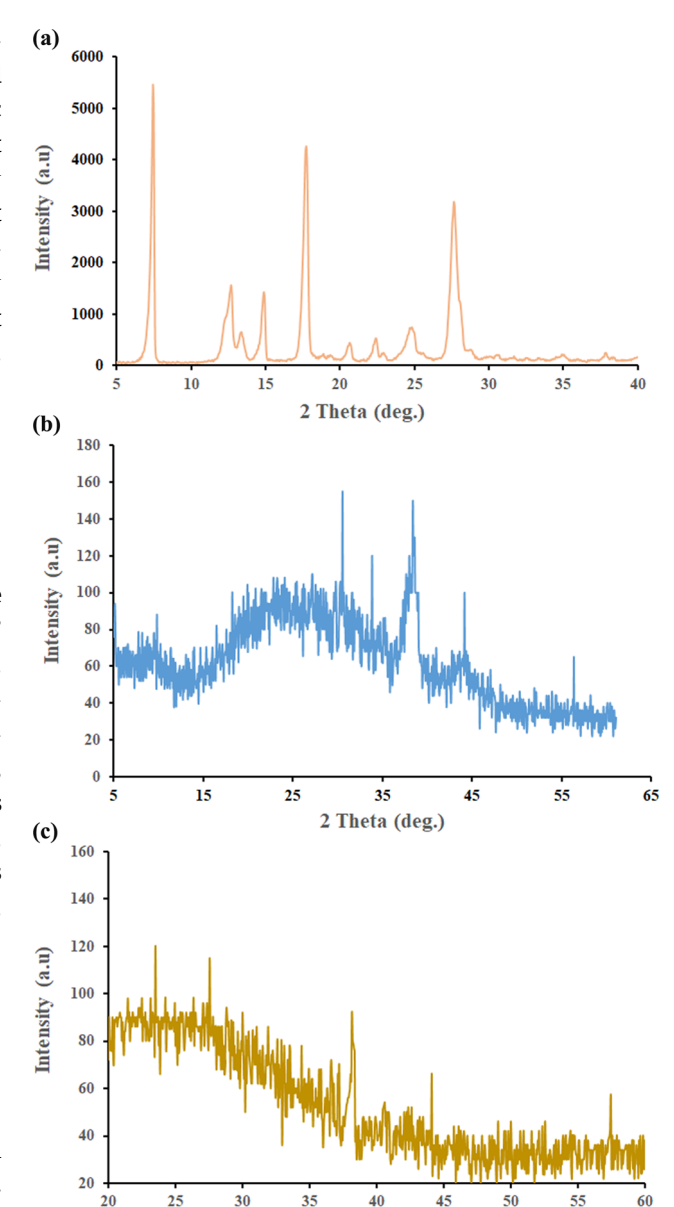


Figure 5: XRD analyses: (a) CHR, (b) AuNPs, and (c) CHR-AuNPs.

2 Theta(deg.)

3.7 Cytotoxicity testing against AMJ13 cell lines

The CHR–AuNPs exhibited higher anti-cancer activity against AMJ13 breast cancer cell lines in comparison to CHR and AuNPs with concentration-dependent cytotoxicity (Figure 8). At 100 μ g/mL CHR–AuNPs concentration, highest 89% cytotoxicity was observed, while at 6.25 μ g/mL, 17% cytotoxicity was observed for the CHR–AuNPs as compared to the control group. The AuNPs treatment

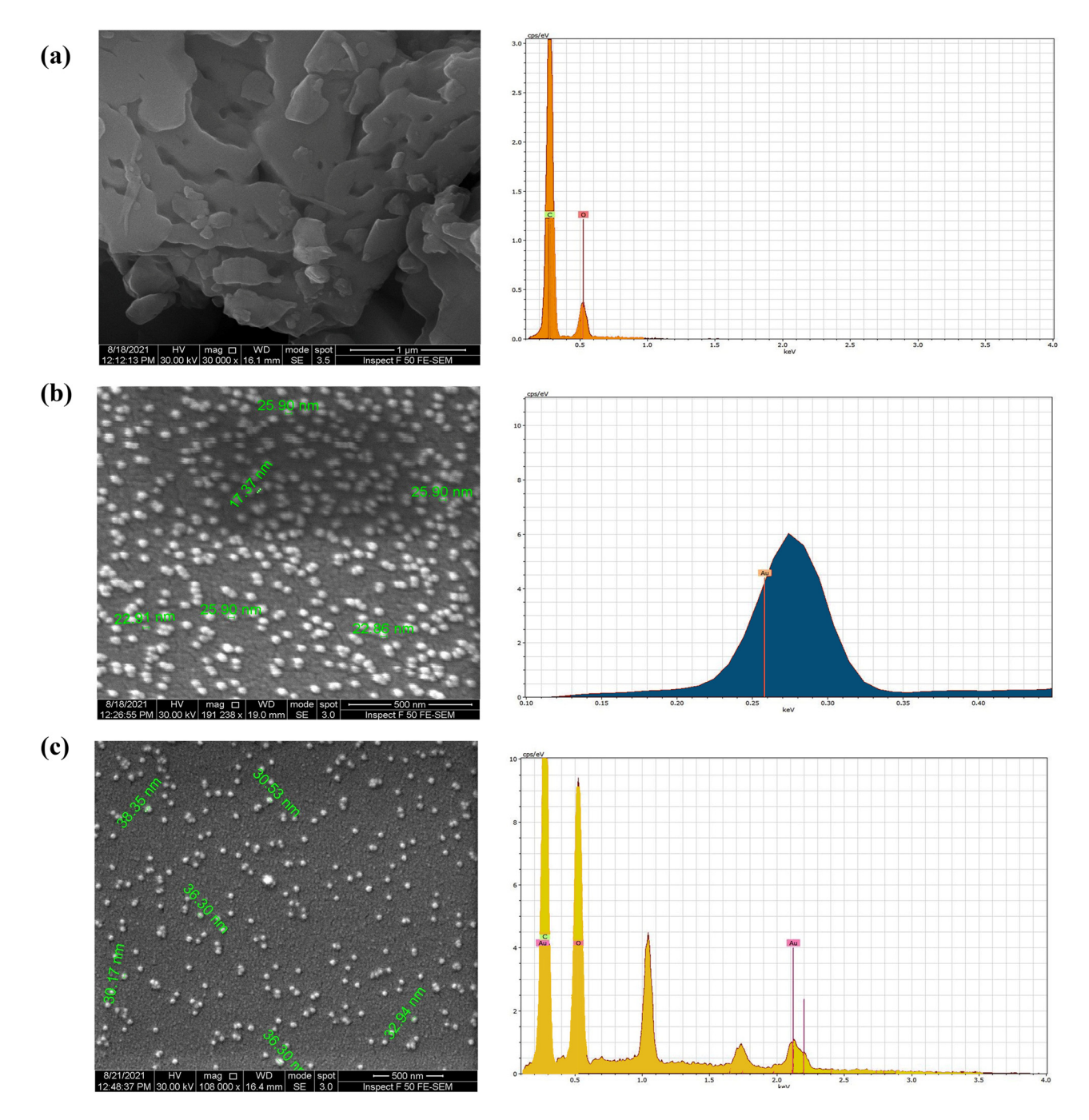


Figure 6: FE-SEM, and energy dispersive analysis (EDX): (a) CHR, (b) AuNPs, and (c) CHR-AuNPs.

was 73.3% effective at $100 \,\mu g/mL$, whereas CHR treatment was 41.5% effective. At 6.25 $\mu g/mL$, AuNPs were effective at 8.9% and CHR was effective at 4.6%.

Crystal violet staining and microscopic examination (Figure 9) demonstrated stronger cytotoxic impacts of CHR-AuNPs against the AMJ13 cell lines. CHR-AuNPs caused cell shape changes, cell size reduction, cell clustering with reduced cell extensions, and shrinkage of nuclei. These changes were absent in non-treated cells (Figure 9).

3.8 Anti-oxidant activity

The anti-oxidant activity of CHR, AuNPs, and CHR-AuNPs, measured at four different concentrations (Figure 10), showed highest free radicals scavenging at 25 µg/mL for all the preparations and the CHR, as compared to the standard, ascorbic acid. The CHR-AuNPs exhibited 91.33% efficacy, while the AuNPs radical scavenging efficiency was 74.89%, and the CHR showed an efficacy of 52.1%.

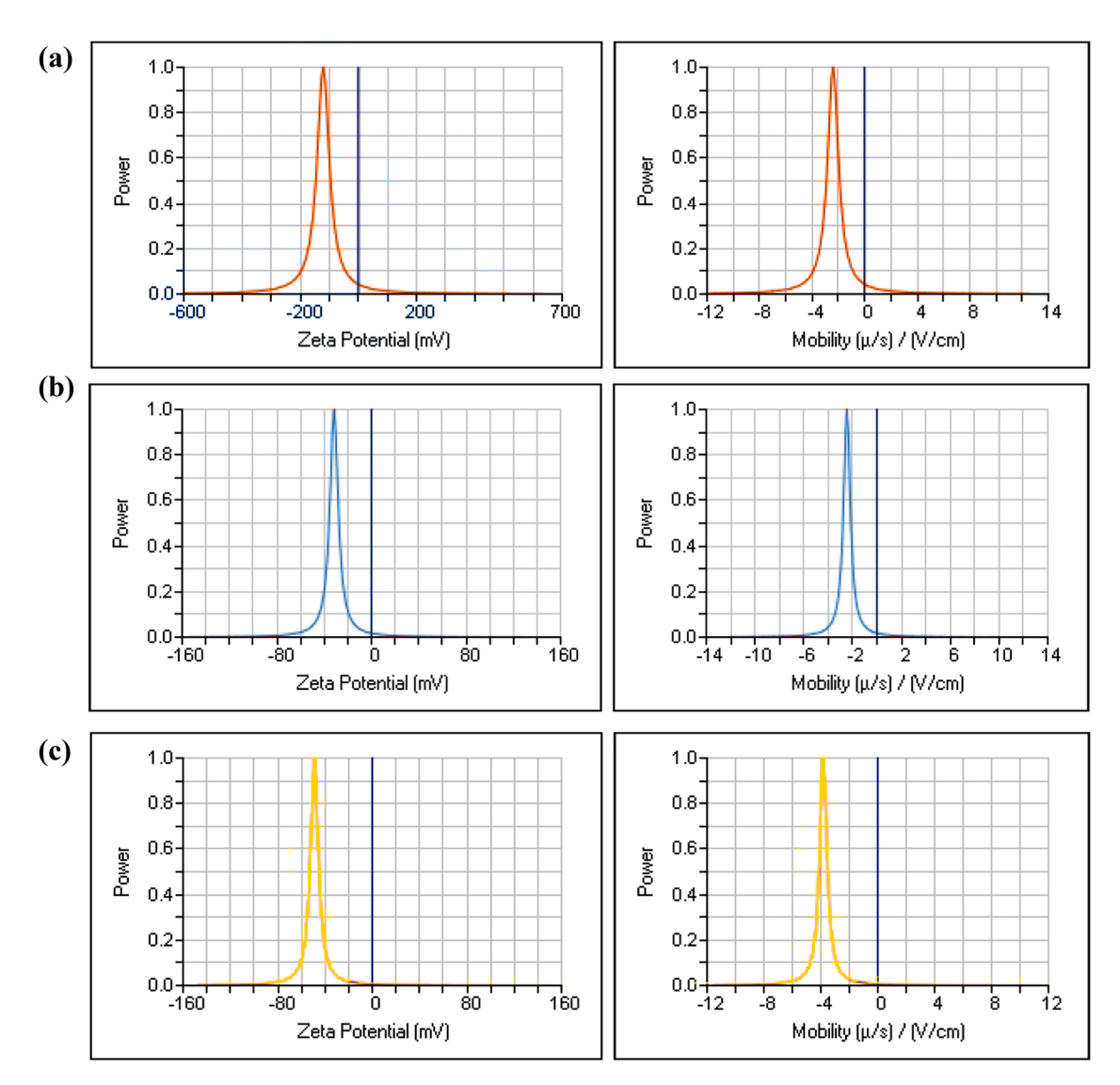


Figure 7: The ζ-potentials: (a) CHR, (b) AuNPs, and (c) CHR-AuNPs.

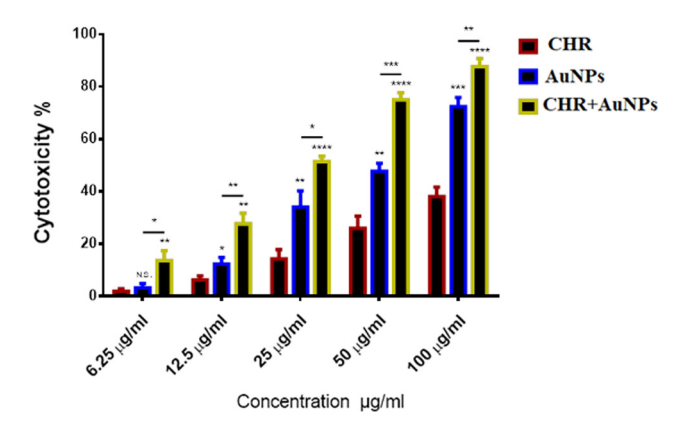


Figure 8: Cytotoxic effects: CHR, AuNPs, and CHR-AuNPs on AMJ13 cell lines; n = 3, N.S., non-significant, *P < 0.05, **P < 0.01, and ****P < 0.001.

The lowest concentration, $3.1\,\mu\text{g/mL}$, showed an efficiency of nearly 15, 25, 30, and 100% for CHR, AuNPs, CHR–AuNPs, and the ascorbic acid, respectively.

3.9 Anti-microbial activities

CHR-AuNPs were found the most effective, and showed highest rate of microbial inhibitions against *S. aureus* and *E. coli* (Figure 11). The inhibition efficiency was followed by AuNPs and CHR which was concentration dependent for all the three preparations, CHR, AuNPs, and CHR-AuNPs.

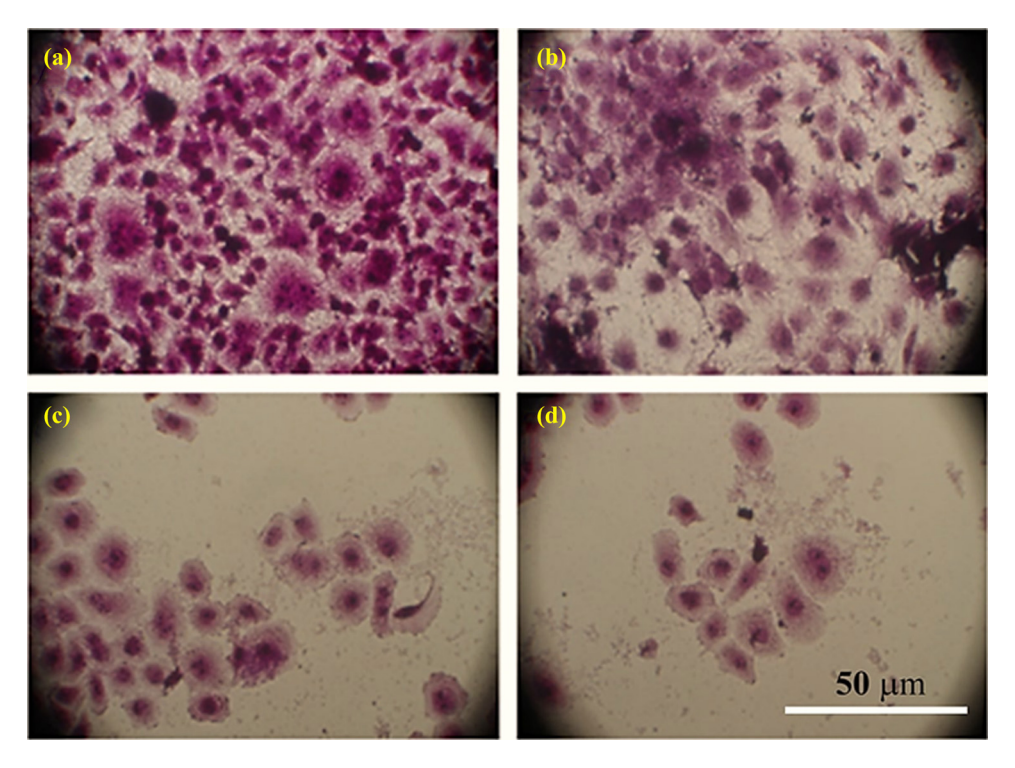


Figure 9: Morphological changes: changes in AMJ13 cell lines stained with crystal violet dye after treatment with CHR, AuNPs, and CHR-AuNPs: (a) non-treated control cells, (b) CHR-treated cells, (c) AuNPs-treated cells, and (d) CHR-AuNPs-treated cells.

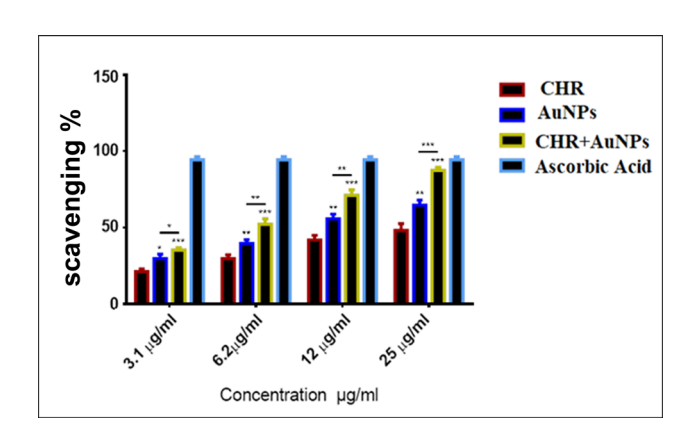


Figure 10: Anti-oxidant activity: CHR-AuNPs, CHR, and AuNPs at different concentrations; n = 3, *P < 0.05, **P < 0.01, and ***P < 0.001.

4 Discussion

CHR, a naturally occurring dihydroxy flavone, is found in passionflower, silver linden, certain geranium species, and is also present in honey and bee propolis [31]. CHR is also used as nutraceutical, and is popular as a supplement for bodybuilding. The compound is used for anxiety, inflammation, gout, HIV/AIDS, erectile dysfunction (ED), and baldness, although no pharmacological evidence has been provided. The compound is also suspected to

increase the male hormone, testosterone, levels. The product is found to protect against neurological changes, improve behavioral patterns, and cognitive functions in Parkinson's disease. It is also anti-inflammatory, anti-neoplastic, anti-oxidant, hepatoprotective, and myosin-light-chain inhibitor in its functions [32,33]. Additionally, CHR has been also reported for its beneficial applications in the treatment of aging, protection against UV_{A^-} and UV_{B^-} induced skin injuries in experimental animals [34,35].

The need for CHR's better formulation, controlled delivery, increments in gut absorptions, and enhanced bioavailability was proposed to overcome the aqueous solubility of the compound. Nanoformulation techniques have been adopted to overcome the comparative increased lipophilicity of this flavonoid product which lacks any glycosidal moiety and is devoid of any hydrophilic substitutions, especially hydroxyl groups, commonly present in majority of flavonoids (Figure 12).

The nanoscale polymeric conjugation, nanoencapsulation, micellar loading, nanoemulsion, aqueous polymeric nanodispersions, cyclodextrin inclusion, nanoliposomes, nanoscale moiety-tagging, and nanometal carriers have been among the important methods to modulate the delivery of the many of the lipophilic products to achieve the therapeutic goals through increased bioavailability, notwithstanding the oral delivery route [36]. The metal

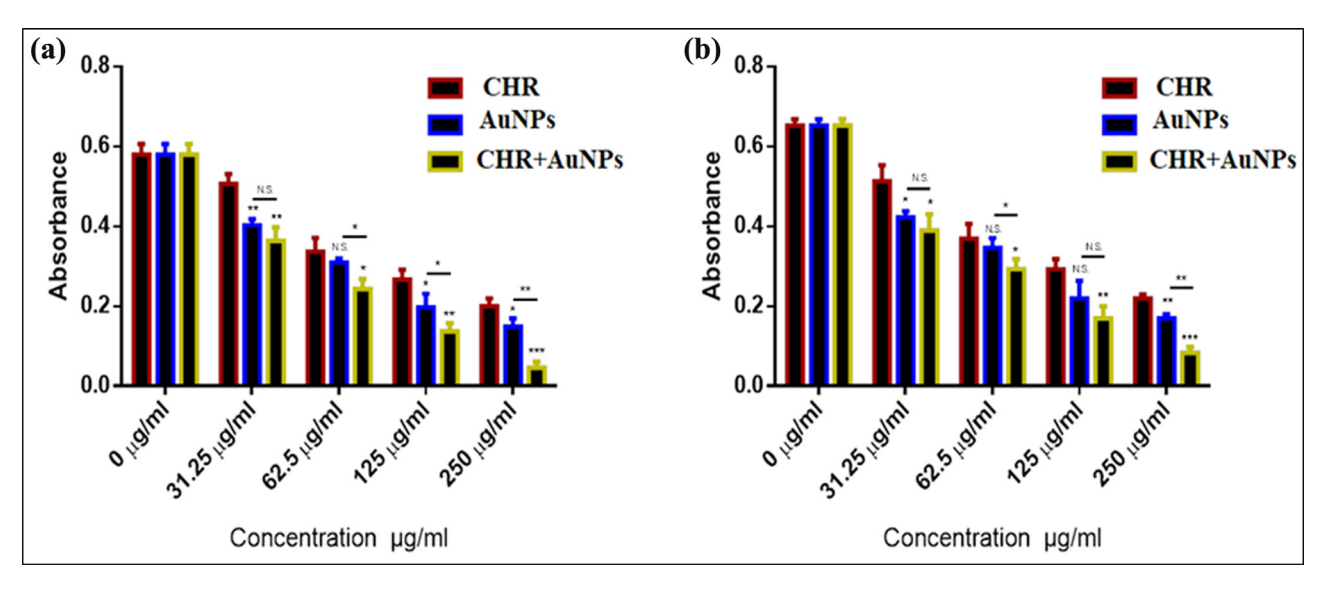


Figure 11: Anti-microbial activity: CHR, AuNPs, and CHR-AuNPs anti-microbial activity against (a) *S. aureus*, (b) *E. coli*. The values represent mean \pm s.d.; n = 3, N.S., non-significant, *P < 0.05, **P < 0.01, and ***P < 0.001.

NP tagging of drugs has provided specific drug targeting, chosen on-site delivery, reduction in toxicity, increased therapeutic efficacy, enhanced safety, biocompatibility, reduced toxicity, and faster development of safe formulations [37]. In this context, the use of gold nanoscale platforms, including gold nanorods, gold nanoclusters, AuNPs,

colloidal gold tagging of drugs, and bio-based entities for therapy and diagnosis have been developed [38]. The AuNPs have proved to be inert, safe, least toxic, tunable, mostly monodisperse nature with synthetic protocols welldeveloped to produce size and shape differentiated nanoentities, and flexible to surface modifications. The AuNPs

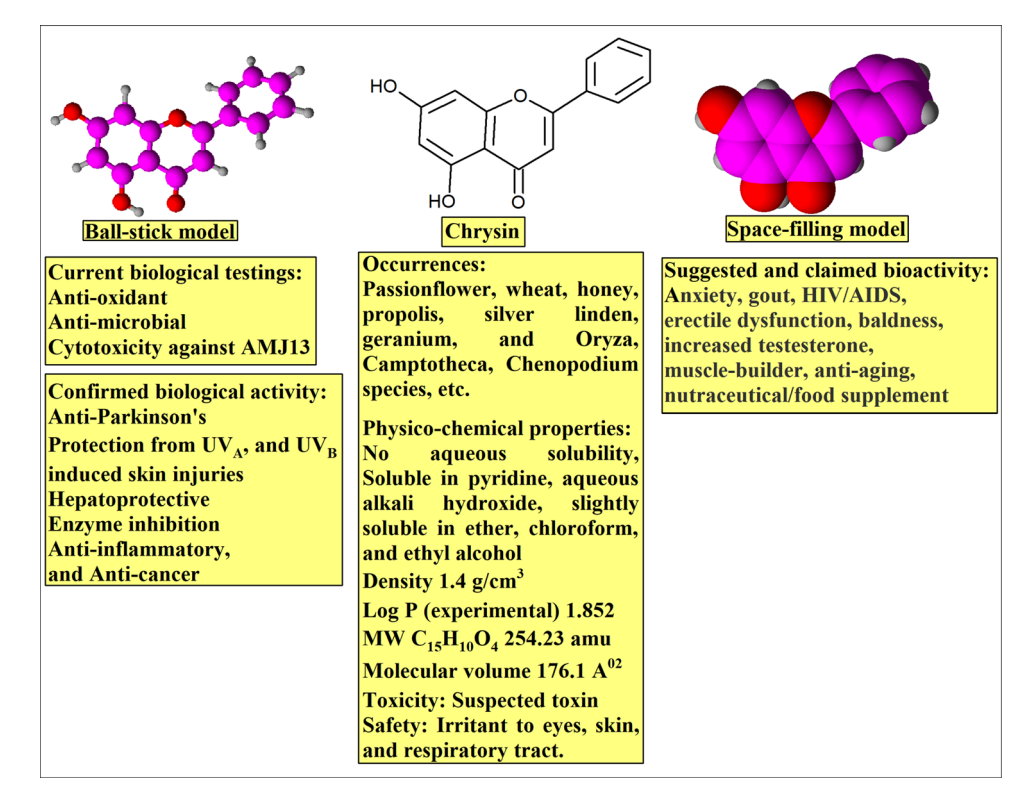


Figure 12: The CHR structure and properties: ball stick, space-filling models, physico-chemical, and biological properties.

tagged drugs are known to resist enzymatic degradation, and have been used to improve poor pharmacokinetics of drugs, its solubility, cancer tissue uptake of the drugs, and can simultaneously engage to adjacent and multiple receptors [39]. Nonetheless, the approach to AuNPs synthesis including the biogenetic, biomimetic, green, environmentally-sustainable, microbial, physical, light amplification by stimulated emission of radiation (LASER), and chemical reduction methods have been developed. Some of these methods have made available the synthesis of AuNPs defining the size, shape, and surface coatings through facile, robust, and quick procedures [40].

The citrate reduction method for producing AuNPs is preferred owing to the ease with which AuNPs can be dispersed in water, and the negative charges of the citrate ions found on the AuNPs surface provide the needed stability to the monodispersed aqueous solution. The reduction of tetrachloroauric acid (HAuCl₄) by citric acid was introduced by Turkevich *et al.* [41] and later modified by Frens [42]. The citrate ions act both as reducing agent and a surface capping agent. The reaction goes without the concern for pH and the particle size decreases with the increase in ratio of the citric acid to the auric acid up to 3.5:1.

The prepared AuNPs also confirmed the surface-plasmonic resonance of the gold metallic NPs and the colorbased observations during the preparation of the AuNPs which exhibited distinct color changes (Figure 1). Moreover, for the cancer cell uptake, NPs under 50 nm have been reported to be allowed access to the cancer cells, where they bind to the cellular sites. Because of their ability to bind to the cell membrane, the AuNPs provide better drug delivery options. The negatively charged citrate coated AuNPs, and the aqueous solution of free chrysin, as examples of gold nanoparticles and molecular entity, are being suggested to provide ionic and hydrophobic interactions, respectively, while the prepared final formulation, gold nanoparticles-conjugated-chrysin, CHR-AuNPs, apparently facilitated the biochemical interactions against the cancer cell lines to produce the cytotoxic effects [43,44]. The present findings indicated that the NPs were stable in solution, as described by the literature [45]. The zeta potential varies depending on the surface charge of dispersion, and higher values imply greater physical stability. At least ±30 mV are required to prevent flocculation and maintain stable dispersion, more than 60 mV confer excellent stability, although value as higher as 100 mV can be obtained. A value of 20 mV confers short-term stability, whereas those ranging between -5 and 5 mV demonstrate fast aggregation [45]. Zeta potential value can also be employed to indicate if the encapsulation of an active, charged material occurs within the center of the NP or on its surface [21].

The UV absorption λ_{\max} change from the AuNPs values at 520 nm, to the CHR-AuNPs at 570 nm demonstrate the ability of the AuNPs to bind to the CHR molecules, wherein the UV absorption λ_{\max} value for the CHR was observed at 268 nm which falls in the UV range, while the absorption change from 520 to 560 nm, of the CHR-AuNPs, falls in the visible range of the spectrum, again demonstrating the plasmon resonance phenomenon, and changes in the optical properties of the CHR-AuNPs, showed the presence of strong CHR, λ_{max} at 268, and the conjugated AuNPs with UV-Vis absorption λ_{max} value at 560 nm (Figure 3). However, several other factors, including particle size, morphology, and probable aggregation determines the absorption maxima [46]. Furthermore, towards establishing the identity of the CHR-AuNPs preparation, the FT-IR spectrum (Figure 4) of CHR, AuNPs, and CHR-AuNPs exhibited characteristic infra-red vibrational absorptions of the constituent functional groups. The OH stretching vibration frequencies of the CHR were found centered at 3012.79 cm⁻¹ indicating the presence of alcoholic functions in the flavonoid structure, while the stretchings at 2929.87, 2713.84, and 2630.91 cm⁻¹ indicated the presence of the aromatic CH bonds, while the α,β -unsaturated carbonyl (C=O) appeared at 1653.00 cm⁻¹. The FT-IR spectrum also indicated the characteristics of an aromatic product with needle-sharp peaks and peaks observed at 840.96 and 731.02 cm⁻¹, the typical aromatic character's absorption peaks. The IR absorptions observed at 3419.79 cm⁻¹ indicated the presence of O-H stretching vibrations, while absorptions at 2987.74 and 2931.80 cm⁻¹ indicated the CH stretching vibrations. The absorption peak at 1583.56, confirmed the presence of C=O group, while the absorption at 1398.39 cm⁻¹ was confirmed for ethereal functionality of the citrate surface AuNPs. The spectrum also displayed non-aromatic characteristics of the product where no aromatic system related absorptions were observed together with non-sharp, somewhat rounded-tip, and lesser peaks. The FT-IR spectrum of CHR-AuNPs showed absorption peak at 3448.72 cm⁻¹ belonging the hydroxyl group (O-H), while the CH stretchings were reflected by the absorptions bands observed at 2960.73 and 2935.66 cm⁻¹. The absorption at $1587.42 \,\mathrm{cm}^{-1}$ for the metal conjugated C=0, at 1463.97 and 1390.68 were attributed to aromatic C-C bonds, and the aromatic C-O stretchings were observed at 1276.88 cm⁻¹. All the CHR, AuNPs, and CHR-AuNPs specific peaks have been observed which exhibited the plausible hydrogen bond, as well as the electrostatic and protonated carbonyl groups' strong associations with the anionic AuNPs [47]. The functional groups IR confirmation, together with the XRD and EDX analyses provided the final conformity to the prepared structure. According to the XRD analysis results obtained, the final product

was confirmed to be molecularly dispersed, and in an amorphous state. Since the CHR coupling interaction did not affect the size of the mineral core, the changes in the NP size, and the observed differences were attributed to the organic envelope of the NP structure [48]. The percentage of carbon and oxygen compositions in the drug-loaded AuNPs was high, thereby confirming that CHR was conjugated with the AuNPs. The anionic nature of the preparations and their size determinations were also obtained from the ζ-potential and the SEM analyses. The high, -30 mV, ζ -potential value confirmed the stable nature of the product (Figure 7) [49]. The surface charge of the NPs also determines the drug's affinity for NPs [50]. The high ζ -potential is also used to interpret the surface attachments of the NPs [51]. The ζ-potential values are also a driving factor for biodistribution [52]. It is a design guide for the rational nanomedicine for providing maximum therapeutic efficacy and bioaccumulation predictability in vivo, where particle size and surface charge controls are critical [53].

The CHR-AuNPs exhibited higher anti-cancer activity against AMJ13 breast cancer cell lines in comparison to CHR and AuNPs with concentration-dependent cytotoxicity (Figure 8). At 100 µg/mL CHR-AuNPs concentration, highest 89% cytotoxicity was observed, while at 6.25 µg/mL, 17% cytotoxicity was observed for the CHR-AuNPs as compared to the control group. The AuNPs treatment was 73.3% effective at 100 µg/mL, whereas CHR treatment was 41.5% effective. At 6.25 µg/mL, AuNPs were effective at 8.9% and CHR was effective at 4.6%. CHR-AuNPs were much more cytotoxic than free CHR, indicating that the anticancer efficacy of CHR has improved since it was functionalized with AuNPs. An overall increase of nearly 18× (85%) was obtained through nanoformulation as compared to the pure CHR.

The concentration of synthetic CHR-AuNPs used in this study was significantly lower than that of CHR. Cell viability decreases as NP concentrations rise, implying that more NPs can be accumulated inside cells, resulting in increased stress, and eventually cell death. The size, shape, surface area, and surface actuations affect NPs biokinetics and toxicity. The CHR-AuNPs inhibited cell proliferation and growth in human breast cancer cell lines, AMJ13, in a concentration-dependent manner (P < 0.05). The CHR-AuNPs showed stronger cytotoxic effects than CHR, indicating that nano-based CHR is better bioavailable, more outreached to the cancer cell lines, and co-activated in conjugation with the AuNPs. Although the concentration of CHR-AuNPs used in this study was much lower than that of the pure CHR, the decreased cell viability observed as the CHR-AuNPs concentration increased,

indicated that more NPs were able to accumulate within cells, and thereby putting stress to the cells, and consequently killing them. The cell death rates were dose-dependent, which could be because of the apoptosis, or necrotic activity, and that would be interesting to investigate the mechanism of cancer cells death.

The cytotoxic effects of CHR, AuNPs, and CHR-AuNPs as shown in AMJ13 cancer cell lines were also proved by the crystal violet staining and the microscopic examination after 24 h of the dose-delivery (Figure 9). The CHR-AuNPs demonstrated stronger cytotoxic impacts against the AMJ13 cell lines. The results prove that CHR-AuNPs caused several impacts. such as changes in the cells shape, reduction in cells sizes, clustering of the cancer cells with a reduced number of cell extensions, suggestive suppressed inter-cellular communications, and shrinking of the nuclei. However, these impacts were absent in non-treated cells (Figure 9). The observations confirmed the cytotoxic activity of the CHR-AuNPs conclusively against human breast cancer cell lines AMJ13.

The anti-oxidant potentials of the CHR, AuNPs, and CHR-AuNPs were observed at 1.3, 2.6, 12.5, and 25 μ g/mL, which revealed that the CHR significantly reduced the levels of DPPH free radicals in a concentration-dependent manner, with 25 µg/mL concentration performing significantly better than the other concentrations (Figure 10). The CHR-AuNPs were found to have higher, 91.33%, ability to quench the DPPH radicals than the CHR and AuNPs which showed 51.2 and 74.89% anti-oxidant activity as compared to the control ascorbic acid, which can be attributed to the increased surface energy and the catalytic potential of the CHR-AuNPs'. The anti-oxidants can donate electrons to the reactive radicals, and convert them to stable, non-reactive forms [54]. The anti-oxidant potential also resumed importance owing to the observations that the free radicals biology has been known to involve in the pathogenesis of several diseases, including cancers. The high anti-oxidant potential of the CHR-AuNPs preparation is in accordance with the increased cytotoxic effects of the preparation in comparison to the anti-oxidant potentials of the CHR and the AuNPs, and their cytotoxic effects.

The nano-CHR, CHR-AuNPs, was also more effective as an anti-microbial preparation, and showed higher rates of microbial inhibitions against microbial isolates, S. aureus and E. coli, which were observed after treatment with different concentrations, 25.31, 62.5, 125, and 250 µg/mL, of the preparation of CHR-AuNPs (Figure 11), and the antimicrobial activity was found to be concentration -dependent. The CHR-AuNPs exhibited highest anti-microbial inhibition rate, much higher than the AuNPs and pure CHR, thereby indicating that the pure CHR improved its anti-microbial efficacy when conjugated with the AuNPs. In addition, the AuNPs showed moderate anti-microbial properties, while the flavonoid CHR showed lesser anti-microbial activity.

The anti-microbial activity against the Gram-positive and Gram-negative bacteria, S. aureus and E. coli, respectively, followed similar patterns of the dose-dependent activity elicitations. The concentration of CHR on the AuNPs surface may have increased their ability to inhibit the bacteria. The mechanisms of microbial inhibitions have been reported to include several pathways, and activities including inhibition of DNA synthesis, alteration of cytoplasmic membrane functions, inhibition of energy metabolism, ligand reductions of the cells, formation of biofilms, inhibition of purines on the cell membrane, alteration of membrane permeability, and damage to the cytoplasmic membrane. The anti-microbial activity of NPs has been studied against Bacillus subtilis, S. aureus, Pseudomonas aeruginosa, Campylobacter jejuni, and E. coli. The Gram-negative microbial strains have thin peptidoglycan layer, and an outer lipopolysaccharide membrane, which is a barrier to cell entry of the negatively charged reactive oxygen species (ROS) [55], while the Gram-positive bacteria allowed entry of negatively charged ROS. Moreover, the anti-microbial activity of NPs is dependent on the particle size. It was demonstrated that decreasing the particle size of the NPs resulted in enhancing the anti-microbial activity [56]. Jones et al. [57] compared the activity MgO, TiO₂, Al₂O₃, CuO, CeO₂, and ZnO NPs against S. aureus. Their results demonstrated that the ZnO NPs showed significant anti-microbial activity. The activity was size dependent and differently-sized ZnO NPs were used in the ranges of >1 µm, 8 nm, and 50-70 nm. Their results confirmed that the small-sized, 8 nm of ZnO NPs was the best in terms of anti-microbial activity. In addition, some studies also referred to the toxicity mechanism of the metal oxide NPs against microbial strains which was also related to their size, morphology, and electrostatic attractions [58]. However, another study reported by Jiang et al. [59] suggested that the NPs affinity to aggregate and attach to the microbial surface may also contribute to NPs toxicity. Additionally, Aruoja et al. [60] suggested that the bactericidal effects of NPs might be specific to the type of metal oxide NPs, and it is a well-known fact that the metallic ions NPs have high affinity for electronrich molecules, such as, the genetic material DNA. Moreover, Jose et al. [61] demonstrated that the NPs could interact with the isolated DNA molecules, and also cause a dose-dependent degradation.

5 Conclusions

The CHR-AuNPs were prepared through simple and efficient chemical method of AuNPs synthesis, and the AuNPs conjugation to the CHR molecules was carried out. The products' physico-chemical characterizations and preliminary trial of biological studies were performed on an initial pilot test scale which included the anti-oxidant, anti-microbial, and cytotoxic activity. It was found that the CHR-AuNPs preparation possessed strong cytotoxicity against human breast cancer cell lines, AMJ13, as well as showed strong anti-oxidant potential and significant anti-microbial activity against Gram-positive and Gramnegative microbial strains, S. aureus and E. coli. The CHR-AuNPs has the potential to be used as an effective therapy as well as a co-therapy agent as part of multiple formulations-based treatments to control and combat the breast cancer. However, more experimentations in this regard are suggested.

Acknowledgments: The researchers would like to thank the Deanship of Scientific Research, Qassim University for funding the publication of this project.

Funding information: This research received no external funding.

Author contributions: All authors have accepted responsibility for the entire content of this manuscript and approved its submission.

Conflict of interest: The authors state no conflict of interest.

References

- Coughlin SS, Ekwueme DU. Breast cancer as a global health concern. Cancer Epidemiol. 2009;33:315-8.
- [2] Salavati H, Debbaut C, Pullens P, Ceelen W. Resistance to intraperitoneal drug delivery and heterogeneity of peritoneal metastasis: the role of hydraulic conductivity. Proceedings of the 2nd Congress of the International Society for the Study of Pleura and Peritoneum; 2021.
- Talib WH, Alsayed AR, Barakat M, Abu-Taha MI, Mahmod AI. Targeting drug chemo-resistance in cancer using natural products. Biomedicines. 2021;9:1353.
- [4] Barani M, Mukhtar M, Rahdar A, Sargazi S, Pandey S, Kang M. Recent advances in nanotechnology-based diagnosis and treatments of human osteosarcoma. Biosensors. 2021;11:55.
- Manisekaran R, García-Contreras R, Rasu Chettiar A-D, Serrano-Díaz P, Lopez-Ayuso CA, Arenas-Arrocena MC, et al. 2D nanosheets - a new class of therapeutic formulations against cancer. Pharmaceutics. 2021;13:1803.
- Storti G, Scioli MG, Kim B-S, Terriaca S, Fiorelli E, Orlandi A, et al. Mesenchymal stem cells in adipose tissue and extracellular vesicles in ovarian cancer patients: a bridge toward metastatic diffusion or a new therapeutic opportunity? Cells. 2021;10:2117.

- Aboubakr EM, Mohammed HA, Hassan AS, Mohamed HB, El Dosoky MI, Ahmad AM. Glutathione-loaded non-ionic surfactant niosomes: a new approach to improve oral bioavailability and hepatoprotective efficacy of glutathione. Nanotechnol Rev. 2022;11:117-37.
- Wahab S, Alshahrani MY, Ahmad MF, Abbas H. Current trends and future perspectives of nanomedicine for the management of colon cancer. Eur I Pharmacol. 2021:910:174464.
- [9] Al-Omar MS, Jabir M, Karsh E, Kadhim R, Sulaiman GM, Taqi ZJ, et al. Gold nanoparticles and graphene oxide flakes enhance cancer cells' phagocytosis through granzyme-perforindependent biomechanism. Nanomaterials. 2021;11:1382.
- [10] Campora S, Ghersi G. Smart nanoparticles in biomedicine: an overview of recent developments and applications; 2021.
- [11] Kong F-Y, Zhang J-W, Li R-F, Wang Z-X, Wang W-J, Wang W. Unique roles of gold nanoparticles in drug delivery, targeting and imaging applications. Molecules. 2017;22:1445.
- [12] Kozlowska A, Szostak-Wegierek D. Flavonoids-food sources and health benefits. Rocz Państwowego Zakładu Hig. 2014;65:79-85.
- [13] Mohammed H. Natural and synthetic flavonoid derivatives with potential antioxidant and anticancer activities. 2009.
- [14] Moghadam ER, Ang HL, Asnaf SE, Zabolian A, Saleki H, Yavari M, et al. Broad-spectrum preclinical antitumor activity of chrysin: current trends and future perspectives. Biomolecules. 2020;10:1374.
- [15] Baidya D, Kushwaha J, Mahadik K, Patil S. Chrysin-loaded folate conjugated PF127-F68 mixed micelles with enhanced oral bioavailability and anticancer activity against human breast cancer cells. Drug Dev Ind Pharm. 2019;45:852-60.
- [16] Gnanasekar S, Palanisamy P, Jha PK, Murugaraj J, Kandasamy M, Mohamed Hussain AMK, et al. Natural honeycomb flavone chrysin (5,7-dihydroxyflavone)-reduced graphene oxide nanosheets fabrication for improved bactericidal and skin regeneration. ACS Sustain Chem Eng. 2018;6:349-63.
- [17] Andleeb A, Andleeb A, Asghar S, Zaman G, Tariq M, Mehmood A, et al. A systematic review of biosynthesized metallic nanoparticles as a promising anti-cancer-strategy. Cancers (Basel). 2021;13:2818.
- [18] Azeeze MSTA, Bhupathi SS, Mohammad EB, Kaliannan D, Balasubramanian B, Meyyanathan SN. Biologically synthesized plant-derived nanomedicines and their in vitro-in vivo toxicity studies in various cancer therapeutics: regulatory perspectives. Cancer Nanotheranostics. 2021;2:217-60.
- [19] Zhang J, Li Z, Zheng K, Li G. Synthesis and characterization of size-controlled atomically precise gold clusters. Phys Sci Rev. 2018;3-268.
- [20] Sulaiman GM, Jabir MS, Hameed AH. Nanoscale modification of chrysin for improved of therapeutic efficiency and cytotoxicity. Artif Cells Nanomed Biotechnol. 2018;46:708-20.
- [21] Sulaiman GM, Waheeb HM, Jabir MS, Khazaal SH, Dewir YH, Naidoo Y. hesperidin loaded on gold nanoparticles as a drug delivery system for a successful biocompatible, anti-cancer, antiinflammatory and phagocytosis inducer model. Sci Rep. 2020;10:10.
- [22] Khanna PK, Gaikwad S, Adhyapak PV, Singh N, Marimuthu R. Synthesis and characterization of copper nanoparticles. Mater Lett. 2007;61:4711-4.
- [23] Mohammed HA, Al-Omar MS, El-Readi MZ, Alhowail AH, Aldubayan MA, Abdellatif AAH. Formulation of ethyl cellulose microparticles incorporated pheophytin a isolated from

- suaeda vermiculata for antioxidant and cytotoxic activities. Molecules, 2019:24:24.
- [24] Sagheer OM, Mohammed MH, Ibraheem ZO, Wadi JS, Tawfeeq MF. Synthesis of gamma biguanides butyric acid analogues as HDAC inhibitors and studying their cytotoxic activity. Mater Today Proc. 2021;47:5983-91.
- [25] Robson A-L, Dastoor PC, Flynn J, Palmer W, Martin A, Smith DW, et al. Advantages and limitations of current imaging techniques for characterizing liposome morphology. Front Pharmacol. 2018;9:80.
- [26] Reddy GR, Morais AB, Gandhi NN. 2,2-Diphenyl-1-picrylhydrazyl free radical scavenging assay and bacterial toxicity of protein capped silver nanoparticles for antioxidant and antibacterial applications. Asian I Chem. 2013:25:9249-54.
- [27] Nalubega R, Kabasa JD, Olila D, Kateregga J. Evaluation of antibacterial activity of selected ethnomedicinal plants for poultry in Masaka district, Uganda. Res J Pharmacol. 2011;5:18-21.
- [28] Asghar M, Habib S, Zaman W, Hussain S, Ali H, Saqib S. Synthesis and characterization of microbial mediated cadmium oxide nanoparticles. Microsc Res Tech. 2020;83:1574-84.
- [29] Applerot G, Perkas N, Amirian G, Girshevitz O, Gedanken A. Coating of glass with ZnO via ultrasonic irradiation and a study of its antibacterial properties. Appl Surf Sci. 2009;256:S3-S8.
- [30] Xin Lee K, Shameli K, Miyake M, Kuwano N, Bt Ahmad Khairudin NB, Bt Mohamad SE, et al. Green synthesis of gold nanoparticles using aqueous extract of Garcinia mangostana fruit peels. J Nanomater. 2016;2016.
- [31] Siddiqui A, Badruddeen, Akhtar J, Uddin MSS, Khan MI, Khalid M, et al. A naturally occurring flavone (chrysin): chemistry, occurrence, pharmacokinetic, toxicity, molecular targets and medicinal properties. J Biol Act Prod Nat. 2018;8:208-27.
- [32] Mohammed HA, Ba LA, Burkholz T, Schumann E, Diesel B, Zapp J, et al. Facile synthesis of chrysin-derivatives with promising activities as aromatase inhibitors. Nat Prod Commun. 2011;6(1):31-4.
- [33] Cho H, Yun C-W, Park W-K, Kong J-Y, Kim KS, Park Y, et al. Modulation of the activity of pro-inflammatory enzymes, COX-2 and iNOS, by chrysin derivatives. Pharmacol Res. 2004:49:37-43.
- [34] Shin EK, Kwon H-S, Kim YH, Shin H-K, Kim J-K. Chrysin, a natural flavone, improves murine inflammatory bowel diseases. Biochem Biophys Res Commun. 2009;381:502-7.
- [35] Wu N-L, Fang J-Y, Chen M, Wu C-J, Huang C-C, Hung C-F. Chrysin protects epidermal keratinocytes from UVA-and UVBinduced damage. J Agric Food Chem. 2011;59:8391-400.
- [36] Jeevanandam J, San Chan Y, Danquah MK. Nano-formulations of drugs: recent developments, impact and challenges. Biochimie. 2016;128:99-112.
- [37] Chandrakala V, Aruna V, Angajala G. Review on metal nanoparticles as nanocarriers: current challenges and perspectives in drug delivery systems. Emergent Mater. 2022;1-23.
- [38] Koushki K, Keshavarz Shahbaz S, Keshavarz M, Bezsonov EE, Sathyapalan T, Sahebkar A. Gold nanoparticles: multifaceted roles in the management of autoimmune disorders. Biomolecules. 2021;11:1289.
- [39] Chiu C-F, Fu R-H, Hsu S, Yu Y-HA, Yang S-F, Tsao TC-Y, et al. Delivery capacity and anticancer ability of the berberineloaded gold nanoparticles to promote the apoptosis effect in breast cancer. Cancers (Basel). 2021;13:5317.

- [40] Hammami I, Alabdallah NM. Gold nanoparticles: synthesis properties and applications. J King Saud Univ. 2021;33:101560.
- [41] Turkevich J, Stevenson PC, Hillier J. A study of the nucleation and growth processes in the synthesis of colloidal gold. Discuss Faraday Soc. 1951;11:55-75.
- [42] Frens G. Controlled nucleation for the regulation of the particle size in monodisperse gold suspensions. Nat Phys Sci. 1973;241:20-2.
- [43] Jazayeri MH, Amani H, Pourfatollah AA, Pazoki-Toroudi H, Sedighimoghaddam B. Various methods of gold nanoparticles (GNPs) conjugation to antibodies. Sens Bio-sensing Res. 2016:9:17-22.
- [44] Gao R, Hao Y, Zhang L, Cui X, Liu D, Zhang M, et al. A facile method for protein imprinting on directly carboxyl-functionalized magnetic nanoparticles using non-covalent template immobilization strategy. Chem Eng J. 2016;284:139-48.
- [45] Nakach M, Authelin J-R, Tadros T, Galet L, Chamayou A. Engineering of nano-crystalline drug suspensions: employing a physico-chemistry based stabilizer selection methodology or approach. Int J Pharm. 2014;476:277-88.
- [46] Shamaila S, Zafar N, Riaz S, Sharif R, Nazir J, Naseem S. Gold nanoparticles: an efficient antimicrobial agent against enteric bacterial human pathogen. Nanomaterials. 2016;6:71.
- [47] Park J-W, Shumaker-Parry JS. Structural study of citrate layers on gold nanoparticles: role of intermolecular interactions in stabilizing nanoparticles. J Am Chem Soc. 2014;136:1907-21.
- [48] Fitzpatrick AWP, Debelouchina GT, Bayro MJ, Clare DK, Caporini MA, Bajaj VS, et al. Atomic structure and hierarchical assembly of a cross-β amyloid fibril. Proc Natl Acad Sci. 2013;110:5468-73.
- [49] Kumar A, Dixit CK. Methods for characterization of nanoparticles. Advances in nanomedicine for the delivery of therapeutic nucleic acids. Amsterdam, Netherlands: Elsevier; 2017. p. 43-58.
- [50] Nandhakumar S, Dhanaraju MD, Sundar VD, Heera B. Influence of surface charge on the in vitro protein adsorption and cell cytotoxicity of paclitaxel loaded poly (ε-caprolactone) nanoparticles. Bull Fac Pharmacy, Cairo Univ. 2017;55:249-58.

- [51] Nejat H, Rabiee M, Varshochian R, Tahriri M, Jazayeri HE, Rajadas J, et al. Preparation and characterization of cardamom extract-loaded gelatin nanoparticles as effective targeted drug delivery system to treat glioblastoma. React Funct Polym. 2017;120:46-56.
- [52] Lagaly G, Dékány I. Colloid clay science. Developments in clay science. Amsterdam, Netherlands: Elsevier; 2013. p. 243-345. ISBN 1572-4352.
- [53] Liu Y, Tan J, Thomas A, Ou-Yang D, Muzykantov VR. The shape of things to come: importance of design in nanotechnology for drug delivery. Ther Deliv. 2012;3:181-94.
- Engwa GA. Free radicals and the role of plant phytochemicals as antioxidants against oxidative stress-related diseases. Phytochem Source Antioxidants Role Dis Prev BoD-Books Demand. 2018;7:49-74.
- [55] Russell AD. Similarities and differences in the responses of microorganisms to biocides. J Antimicrob Chemother. 2003;52:750-63.
- [56] Abebe B, Murthy HCA, Zerefa E, Adimasu Y. PVA assisted ZnO based mesoporous ternary metal oxides nanomaterials: synthesis, optimization, and evaluation of antibacterial activity. Mater Res Exp. 2020;7:45011.
- Jones N, Ray B, Ranjit KT, Manna AC. Antibacterial activity of [57] ZnO nanoparticle suspensions on a broad spectrum of microorganisms. FEMS Microbiol Lett. 2008;279:71-6.
- [58] Heinlaan M, Ivask A, Blinova I, Dubourguier H-C, Kahru A. Toxicity of nanosized and bulk ZnO, CuO and TiO2 to bacteria vibrio fischeri and crustaceans daphnia magna and thamnocephalus platyurus. Chemosphere. 2008;71:1308-16.
- [59] Jiang W, Mashayekhi H, Xing B. Bacterial toxicity comparison between nano-and micro-scaled oxide particles. Environ Pollut. 2009;157:1619-25.
- [60] Aruoja V, Dubourguier H-C, Kasemets K, Kahru A. Toxicity of nanoparticles of CuO, ZnO and TiO2 to microalgae pseudokirchneriella subcapitata. Sci Total Environ. 2009;407:1461-8.
- [61] Jose GP, Santra S, Mandal SK, Sengupta TK. Singlet oxygen mediated DNA degradation by copper nanoparticles: potential towards cytotoxic effect on cancer cells. J Nanobiotechnol. 2011;9:1-8.